

# Photoproduction of the $\omega$ meson on the proton near threshold

I. I. Strakovsky,<sup>1,\*</sup> S. Prakhov,<sup>1,2,3,†</sup> Ya. I. Azimov,<sup>4</sup> P. Aguar-Bartolomé,<sup>2</sup> J. R. M. Annand,<sup>5</sup> H. J. Arends,<sup>2</sup> K. Bantawa,<sup>6</sup> R. Beck,<sup>7</sup> V. Bekrenev,<sup>4</sup> H. Berghäuser,<sup>8</sup> A. Braghieri,<sup>9</sup> W. J. Briscoe,<sup>1</sup> J. Brudvik,<sup>3</sup> S. Cherepnaya,<sup>10</sup> R. F. B. Codling,<sup>5</sup> C. Collicott,<sup>11,12</sup> S. Costanza,<sup>9</sup> B. T. Demissie,<sup>1</sup> E. J. Downie,<sup>2,1</sup> P. Drexler,<sup>8</sup> L. V. Fil'kov,<sup>10</sup> D. I. Glazier,<sup>5,13</sup> R. Gregor,<sup>8</sup> D. J. Hamilton,<sup>5</sup> E. Heid,<sup>1,2</sup> D. Hornidge,<sup>14</sup> I. Jaegle,<sup>15</sup> O. Jahn,<sup>2</sup> T. C. Jude,<sup>13</sup> V. L. Kashevarov,<sup>2,10</sup> I. Keshelashvili,<sup>15</sup> R. Kondratiev,<sup>16</sup> M. Korolija,<sup>17</sup> M. Kotulla,<sup>8</sup> A. Koulbardi,<sup>4</sup> S. Kruglov,<sup>4,‡</sup> B. Krusche,<sup>15</sup> V. Lisin,<sup>10</sup> K. Livingston,<sup>5</sup> I. J. D. MacGregor,<sup>5</sup> Y. Maghrbi,<sup>15</sup> D. M. Manley,<sup>6</sup> Z. Marinides,<sup>1</sup> J. C. McGeorge,<sup>5</sup> E. F. McNicoll,<sup>5</sup> D. Mekterovic,<sup>17</sup> V. Metag,<sup>8</sup> D. G. Middleton,<sup>2,14</sup> A. Mushkarenkov,<sup>9</sup> B. M. K. Nefkens,<sup>3,‡</sup> A. Nikolaev,<sup>7</sup> R. Novotny,<sup>8</sup> H. Ortega,<sup>2</sup> M. Ostrick,<sup>2</sup> P. B. Otte,<sup>2</sup> B. Oussena,<sup>1,2</sup> P. Pedroni,<sup>9</sup> F. Pheron,<sup>15</sup> A. Polonski,<sup>16</sup> J. Robinson,<sup>5</sup> G. Rosner,<sup>5</sup> T. Rostomyan,<sup>15</sup> S. Schumann,<sup>2</sup> M. H. Sikora,<sup>1,13</sup> A. Starostin,<sup>3</sup> I. Supek,<sup>17</sup> M. F. Taragin,<sup>1</sup> C. M. Tarbert,<sup>13</sup> M. Thiel,<sup>8</sup> A. Thomas,<sup>2</sup> M. Unverzagt,<sup>2,7</sup> D. P. Watts,<sup>13</sup> D. Werthmüller,<sup>15</sup> and F. Zehr<sup>15</sup>

(A2 Collaboration at MAMI)

<sup>1</sup>The George Washington University, Washington, DC 20052-0001, USA

<sup>2</sup>Institut für Kernphysik, University of Mainz, D-55099 Mainz, Germany

<sup>3</sup>University of California Los Angeles, Los Angeles, California 90095-1547, USA

<sup>4</sup>Petersburg Nuclear Physics Institute, 188300 Gatchina, Russia

<sup>5</sup>SUPA School of Physics and Astronomy, University of Glasgow, Glasgow G12 8QQ, United Kingdom

<sup>6</sup>Kent State University, Kent, Ohio 44242-0001, USA

<sup>7</sup>Helmholtz-Institut für Strahlen- und Kernphysik, University of Bonn, D-53115 Bonn, Germany

<sup>8</sup>II Physikalisches Institut, University of Giessen, D-3539 Giessen, Germany

<sup>9</sup>INFN Sezione di Pavia, I-27100 Pavia, Italy

<sup>10</sup>Lebedev Physical Institute, 119991 Moscow, Russia

<sup>11</sup>Dalhousie University, Halifax, Nova Scotia B3H 4R2, Canada

<sup>12</sup>Saint Marys University, Halifax, Nova Scotia B3H 3C3, Canada

<sup>13</sup>School of Physics, University of Edinburgh, Edinburgh EH9 3JZ, United Kingdom

<sup>14</sup>Mount Allison University, Sackville, New Brunswick E4L 1E6, Canada

<sup>15</sup>Institut für Physik, University of Basel, CH-4056 Basel, Switzerland

<sup>16</sup>Institute for Nuclear Research, 125047 Moscow, Russia

<sup>17</sup>Rudjer Boskovic Institute, HR-10000 Zagreb, Croatia

(Dated: December 6, 2024)

An experimental study of  $\omega$  photoproduction on the proton was conducted by using the Crystal Ball and TAPS multiphoton spectrometers together with the photon tagging facility at the Mainz Microtron MAMI. The  $\gamma p \rightarrow \omega p$  differential cross sections are measured from threshold to the incident-photon energy  $E_\gamma = 1.40$  GeV ( $W = 1.87$  GeV for the center-of-mass energy) with 15-MeV binning in  $E_\gamma$  and full production-angle coverage. The quality of the present data near threshold gives access to a variety of interesting physics aspects. As an example, an estimation of the  $\omega N$  scattering length  $\alpha_{\omega p}$  is provided.

PACS numbers: 12.40.Vv, 13.60.Le, 14.40.Be, 25.20.Lj

## I. INTRODUCTION

Although Quantum Chromodynamics (QCD) is generally believed to govern strong interactions, it still can be applied to particular problems only in terms of specific model-dependent approaches, which can be distinguished by their predictions for the resonance spectra. However, such predictions can only be verified in collisions of a very restricted set of hadron pairs: a proton or a bound neutron as a target and a stable or a weakly decaying hadron as a projectile. Meanwhile, various constituent quark

models (e.g., see Ref. [1] and references therein) predict a richer spectrum of hadron resonances than have so far been observed in experiments [2]. Because most known baryon states were discovered in elastic  $\pi N$  scattering, some resonances could have been missed because of their weak coupling to the  $\pi N$  channels [3]. At the same time, a stronger coupling of those resonances to such channels as  $\eta N$ ,  $\omega N$ ,  $K\Lambda$ , or  $K\Sigma$  cannot be excluded, and, therefore, an extensive study of these channels is very important in searching for the so-called “missing” resonances [4]. Proof of their existence would constitute a strong confirmation of the validity of the constituent quark concept.

Although the  $\omega$  meson is neither stable nor decaying weakly, the  $\omega N$  channel is favorable in searching for missing resonances because, owing to vector-meson dominance (VMD) [5],  $\omega$  photoproduction on the nu-

\*corresponding author, e-mail: igor@gwu.edu

†corresponding author, e-mail: prakhov@ucla.edu

‡deceased

cleon may be directly related to the elastic amplitude for  $\omega N$  scattering. In addition,  $\omega$  photoproduction provides an “isospin filter” for the nucleon response because  $\omega N$  final states can originate only from  $N^*$  states with  $I = 1/2$ , but not from  $\Delta^*$ s with  $I = 3/2$ . The  $\omega N$  threshold region is also especially attractive in searching for new resonances because the reaction threshold is located at the higher-energy edge of the third resonance region, in which the Review of Particle Physics (RPP) [2] shows seven  $N^*$  states with masses between 1650 and 1720 MeV, and then there are no observed  $N^*$  states up to 1860 MeV. It cannot be excluded that this energy range may contain unknown  $N^*$  resonances that are coupled more strongly to  $\omega N$  than to other meson-baryon channels. Such a strong coupling to resonances in the near-threshold region is clearly seen, for example, for the two most dominant channels,  $\pi N$  and  $\eta N$ , coupled to  $\Delta(1232)3/2^+$  and  $N(1535)1/2^-$ , respectively.

The photoproduction of  $\omega$  mesons was under extensive theoretical discussion since the first high-statistics differential cross sections and polarization results were provided from SAPHIR [6], covering a broad interval in center-of-mass (c.m.) energy, up to  $W = 2.4$  GeV with  $\sim 60\%$  of the full production-angle range. Many models, including coupled channel, effective Lagrangian, and QCD-inspired approaches [7–12], were developed, trying to explain the behavior of the experimental data. Another high-statistics measurement of the  $\gamma p \rightarrow \omega p$  differential cross sections and spin-density matrix elements was recently made by the CLAS Collaboration [13], covering c.m. energies from threshold up to  $W = 2.84$  GeV. Their binning in c.m. energy was much finer than from SAPHIR [6], but the production-angle coverage was narrower. Unfortunately, for both SAPHIR and CLAS, the data obtained in the energy region near threshold have the poorest quality.

Both SAPHIR [6] and CLAS [13] experiments measured the photoproduction of  $\omega$  via its major decay mode  $\omega \rightarrow \pi^+\pi^-\pi^0$ , having 89.2% branching ratio [2]. The analyses of those experimental data were challenging because of large background from  $\gamma p \rightarrow \pi^+\pi^-\pi^0 p$  produced via intermediate states different from  $\gamma p \rightarrow \omega p$ . In the analysis by SAPHIR [6], all data points were obtained by individual fits of the  $\omega$  peak above the  $\pi^+\pi^-\pi^0$  background. Their fitting procedure experienced difficulties with describing the  $\omega$  peak near threshold as a standard Breit-Wigner (BW) shape was severely distorted by phase space, and a function (BW with parameters of  $\omega$  convoluted with two Gaussians describing the experimental resolutions) used for higher energies did not work here. In the analysis by CLAS [13], a so-called  $Q$ -factor technique was used to separate signal and background events, allowing to fit data with the event-by-event approach and to extract all results from their unbinned maximum-likelihood fits.

A background contamination of  $\omega$  events would be expected to improve if  $\omega$  photoproduction were measured in process  $\gamma p \rightarrow \omega p \rightarrow \pi^0 \gamma p \rightarrow 3 \gamma p$ , using a radiative decay mode,  $\omega \rightarrow \pi^0 \gamma$ , with 8.28% branching ratio [2].

Other physical processes having the three-photon final state are expected to be very small. However, as shown in a preliminary analysis of the CBELSA/TAPS data [14], the three-photon background can come from processes  $\gamma p \rightarrow \pi^0 \pi^0 p \rightarrow 4 \gamma p$  and  $\gamma p \rightarrow \pi^0 \eta p \rightarrow 4 \gamma p$  when one of the four final-state photons was not detected.

In this work, a new high-statistics measurement of the  $\gamma p \rightarrow \omega p$  differential cross sections near threshold is presented. The results are based on an analysis of  $\sim 5 \times 10^5$   $\omega$  mesons detected via their  $\pi^0 \gamma$  decay mode. All data were divided into 20 (15 MeV each) bins in the incident-photon energy,  $E_\gamma$ , and 15 angular bins, covering the full range of the  $\omega$  production angle. All results are obtained by individual fits of the  $\omega$  peak above background in each energy-angle bin.

A partial-wave analysis with extracting spin-density matrix elements from the present data is in progress, by using the  $Q$ -factor technique. As the latter analysis is being performed by a theoretical group outside the A2 Collaboration, their results will be published later on separately.

## II. EXPERIMENTAL SETUP

The process  $\gamma p \rightarrow \omega p \rightarrow \pi^0 \gamma p \rightarrow 3 \gamma p$  was measured using the Crystal Ball (CB) [15] as a central spectrometer and TAPS [16, 17] as a forward spectrometer. These detectors were installed at the energy-tagged bremsstrahlung-photon beam produced from the electron beam of the Mainz Microtron (MAMI) [18, 19]. In the present experiment, bremsstrahlung photons, produced by the 1508-MeV electrons in a 10- $\mu$ m Cu radiator and collimated by a 4-mm-diameter Pb collimator, were incident on a 5-cm-long liquid-hydrogen (LH<sub>2</sub>) target located in the center of the CB. The energies of the incident photons were analyzed up to 1402 MeV by detecting the postbremsstrahlung electrons in the Glasgow tagging spectrometer (or tagger) [20–22]. The uncertainty in the energy of the tagged photons is mainly determined by the width of tagger focal-plane detectors and the energy of the MAMI electron beam used in experiments. For the MAMI energy of 1508 MeV, such an uncertainty was about  $\pm 2$  MeV.

The CB detector is a sphere consisting of 672 optically isolated NaI(Tl) crystals, shaped as truncated triangular pyramids, which point toward the center of the sphere. The crystals are arranged in two hemispheres that cover 93% of  $4\pi$  sr, sitting outside a central spherical cavity with a radius of 25 cm, which is designed to hold the target and inner detectors. In this experiment, TAPS was arranged in a plane consisting of 384 BaF<sub>2</sub> counters of hexagonal cross section. It was installed 1.5 m downstream of the CB center and covered the full azimuthal range for polar angles from  $1^\circ$  to  $20^\circ$ .

The experimental trigger required the total energy deposited in the CB to exceed  $\sim 320$  MeV and the number of so-called hardware clusters in the CB (multiplicity trigger) to be two or larger. In the trigger, a hardware cluster

in the CB was a block of 16 adjacent crystals in which at least one crystal had an energy deposit larger than 30 MeV. The TAPS information was not used in the trigger of the present experiment.

More details on the experimental setup, its resolutions, and other conditions during the period of the data taking (first half of 2007) are given in Refs. [23, 24] and references therein.

### III. DATA HANDLING

The reaction  $\gamma p \rightarrow \omega p$  was searched for in events identified as  $\gamma p \rightarrow \pi^0 \gamma p \rightarrow 3\gamma p$  candidates, having three or four clusters reconstructed in the CB and TAPS together by software analysis. The cluster algorithm in software was optimized for finding a group of adjacent crystals in which the energy was deposited by a single-photon electromagnetic shower. This algorithm also works well for a proton cluster. The software threshold for the cluster energy was chosen to be 12 MeV. For the  $\gamma p \rightarrow \pi^0 \gamma p \rightarrow 3\gamma p$  candidates, the three-cluster events were analyzed assuming that the final-state proton was not detected. This typically happens when the outgoing proton is stopped in the material of the downstream beam tunnel of the CB, or the proton scatters in the backward direction within the c.m. frame, resulting in such a low kinetic energy of the proton in the laboratory system that it is below the software cluster threshold. Thus, including three-cluster events in the analysis is vital for measuring  $\gamma p \rightarrow \omega p$  differential cross sections at very forward production angles of  $\omega$ . The fraction of  $\gamma p \rightarrow \omega p \rightarrow \pi^0 \gamma p \rightarrow 3\gamma p$  events without the detected proton varies from 2.7% at the reaction threshold to 7.6% at the highest energy of the present experiment.

The selection of event candidates and the reconstruction of the reaction kinematics was based on the kinematic-fit technique. Details on the kinematic-fit parametrization of the detector information and resolutions are given in Ref. [24]. As discussed there, the information for the outgoing proton, if it is detected, is used in the kinematic fit without the proton kinetic energy, which has large uncertainties because of the material between the target and the crystals of the calorimeters. In addition, when energetic protons punch through the crystals, their kinetic energy cannot be determined from their energy deposit. For three-clusters events, all parameters of the outgoing proton are free variables of the kinematic fit. All three- and four-clusters events that satisfied the  $\gamma p \rightarrow \pi^0 \gamma p \rightarrow 3\gamma p$  hypothesis with a probability greater than 2% were accepted for further analysis. The kinematic fitting for this hypothesis includes the four main constraints, which are based on the conservation of energy and three-momentum, and an additional constraint on the invariant mass of two outgoing photons to have the  $\pi^0$ -meson mass. The kinematic-fit output was used to reconstruct the kinematics of the outgoing particles. Small misidentification of the proton with a photon for the selected  $\gamma p \rightarrow \omega p \rightarrow \pi^0 \gamma p \rightarrow 3\gamma p$  events was observed

only in the three-clusters events and only for clusters reconstructed in TAPS. Such events were discarded based on the time of flight between a TAPS cluster and the CB signal with respect to the energy of the TAPS cluster.

The determination of the experimental acceptance was based on a Monte Carlo (MC) simulation of  $\gamma p \rightarrow \omega p \rightarrow \pi^0 \gamma p$  with an isotropic production-angular distribution and an uniform beam distribution generated from the reaction threshold up to the maximal experimental energy. To reproduce the energy dependence of the  $\omega$  resonance shape near production threshold, the reaction  $\gamma p \rightarrow \pi^0 \gamma p$  was generated first as phase space. Then, the invariant mass of the  $\pi^0 \gamma$  system,  $m(\pi^0 \gamma)$ , was folded with the Breit-Wigner (BW) function, the parameters of which were taken for the  $\omega$  meson ( $m = 782.65$  MeV and  $\Gamma = 8.49$  MeV) from the RPP [2]. This approach allowed one to properly reproduce the folding of the BW shape with phase space. All MC events were propagated through a GEANT (3.21) simulation of the experimental setup. To reproduce resolutions of the experimental data, the GEANT output was subject to additional smearing, thus allowing both the simulated and experimental data to be analyzed in the same way. Matching the energy resolution between the experimental and MC events was adjusted via reaching agreement in the invariant-mass resolutions and in the kinematic-fit stretch functions (or pulls) and probability distributions. Such an adjustment was based on the analysis of the same data set for reactions having almost no physical background (namely,  $\gamma p \rightarrow \pi^0 p$ ,  $\gamma p \rightarrow \eta p \rightarrow \gamma \gamma p$ , and  $\gamma p \rightarrow \eta p \rightarrow 3\pi^0 p$  [24]). After taking into account the trigger requirements in the analysis of the MC events, the average acceptance for the process  $\gamma p \rightarrow \omega p \rightarrow \pi^0 \gamma p$  in the A2 experimental setup was found to be about 50%. The simulation of the trigger was adjusted with the same reactions that was used for adjusting the energy resolution, where  $\gamma p \rightarrow \pi^0 p$  and  $\gamma p \rightarrow \eta p \rightarrow \gamma \gamma p$  are especially sensitive to the multiplicity trigger, required two hardware clusters in the CB. The agreement of the  $\gamma p \rightarrow \eta p$  differential cross sections obtained from both the  $\eta \rightarrow \gamma \gamma$  and the  $\eta \rightarrow 3\pi^0$  decay modes was another cross-check for the correctness of the trigger simulation. As found out, the multiplicity trigger was not important for the present analysis, as all  $\gamma p \rightarrow \omega p \rightarrow \pi^0 \gamma p$  events that passed the requirement on the CB total energy to exceed 320 MeV had more than one hardware cluster in the CB.

As turned out, the selected experimental events with  $\omega \rightarrow \pi^0 \gamma$  decays were also contaminated with some background distributed quite smoothly under the  $\omega$  peak. Based on the MC simulations of possible background reactions, it was found that processes  $\gamma p \rightarrow \pi^0 \pi^0 p \rightarrow 4\gamma p$  and  $\gamma p \rightarrow \pi^0 \eta p \rightarrow 4\gamma p$  could mimic  $\gamma p \rightarrow \pi^0 \gamma p$  when one of the four final-state photons had not been detected. The background from these processes mostly contaminates the four-cluster events. Events from reaction  $\gamma p \rightarrow \pi^0 \pi^+ n$  can mimic  $\gamma p \rightarrow \pi^0 \gamma p$  when the outgoing neutron was not detected, and they contaminate the three-cluster events. Nevertheless, there was no background process found that could mimic the  $\omega \rightarrow \pi^0 \gamma$

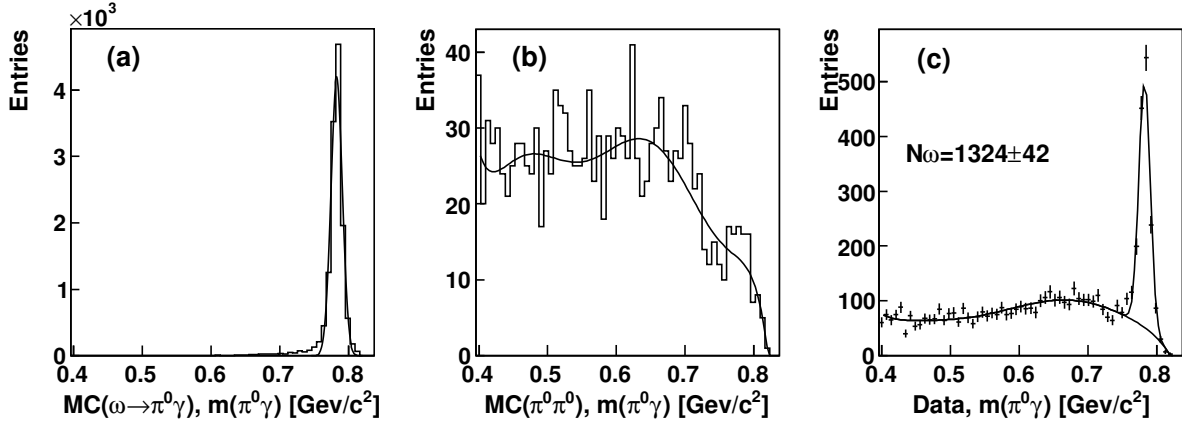


FIG. 1:  $m(\pi^0\gamma)$  invariant-mass distributions obtained for  $E_\gamma = 1176$  MeV and  $\cos\theta = 0$ . (a) MC simulation of  $\gamma p \rightarrow \omega p \rightarrow \pi^0\gamma p$  with a Gaussian fit ( $\sigma = 8.2$  MeV and FWHM = 19.3 MeV). (b) MC simulation of the background reaction  $\gamma p \rightarrow \pi^0\pi^0 p$  fitted with a polynomial of order eight. (c) Measured spectrum fitted with the sum of a Gaussian and a polynomial of order eight, where  $N_\omega$  is the number of  $\omega$  mesons found from this fit.

peak.

Because the suppression of the background processes was not possible without severe losses in  $\omega \rightarrow \pi^0\gamma$  events themselves, and the subtraction of the background processes was not possible without precise MC simulations of all possible background reactions, the  $\omega \rightarrow \pi^0\gamma$  events were measured by fitting experimental  $m(\pi^0\gamma)$  spectra with some function, describing the  $\omega$  peak above a smooth background. To measure the  $\gamma p \rightarrow \omega p$  differential cross sections, all events were divided into 20 incident-photon energy bins from the reaction threshold to  $E_\gamma = 1402$  MeV. The data within each energy bin were divided into 15 identical  $\cos\theta$  bins, covering the full range from -1 to 1, where  $\theta$  was the angle between the directions of the outgoing  $\pi^0\gamma$  system and the incident photon in the c.m. frame. The number of  $\omega \rightarrow \pi^0\gamma$  decays observed in each energy-angle bin was determined by an individual fit of the corresponding  $m(\pi^0\gamma)$  spectra.

The fitting procedure for one energy-angle bin is illustrated in Figs. 1-3, showing typical changes in the shape of the  $\omega$  peak and the background depending on  $\theta$  and  $E_\gamma$ . Panels (a) in these figures depict the  $m(\pi^0\gamma)$  distributions for the MC simulation of  $\gamma p \rightarrow \omega p \rightarrow \pi^0\gamma p$  fitted with a Gaussian. The choice of the normal distribution for the fitting procedure is motivated by the facts that the BW shape of the  $\omega$  peak is severely cut by phase space near threshold and the  $m(\pi^0\gamma)$  resolution strongly dominates the  $\omega$ -meson width ( $\Gamma = 8.49$  MeV [2]), especially for the very forward production angles of  $\omega$ . Because the outgoing proton is not detected for those angles, it is treated as a missing particle in the kinematic fit, resulting in a poorer  $m(\pi^0\gamma)$  resolution for the three-cluster events. In the case of the Gaussian fits shown in panels (a), the full width at half maximum (FWHM) increases from 19.3 MeV for  $E_\gamma = 1176$  MeV and  $\cos\theta = 0$  to 29.2 MeV for  $\cos\theta = 0.93$  at the same energy, and to 32.0 MeV for  $E_\gamma = 1325$  MeV and the same angular bin.

Panels (b) in these three figures show the  $m(\pi^0\gamma)$  distributions for the MC simulation of  $\gamma p \rightarrow \pi^0\pi^0 p$ , which is

one of the background processes. The reaction itself was generated as  $\gamma p \rightarrow \pi^0\Delta^+(1232) \rightarrow \pi^0\pi^0 p$ . The production angular distribution of  $\gamma p \rightarrow \pi^0\Delta$  and the rest-frame  $\Delta^+(1232) \rightarrow \pi^0 p$  decay distribution with respect to the  $\Delta$ 's directions were also generated isotropically. A more precise generation of the reaction kinematics were unnecessary as these spectra were used only for obtaining initial values for parameters of the function describing the experimental background.

To separate the  $\omega$  signal from the background, the experimental  $m(\pi^0\gamma)$  distributions were fitted with the sum of a Gaussian, describing the  $\omega$  peak, and a polynomial, describing the background. These fits are shown in panels (c). The order of the polynomial was chosen to be sufficient for a fairly good description of the background distribution in the range  $m(\pi^0\gamma) > 0.4$   $\text{GeV}/c^2$ . Typically, there was no need to use a polynomial higher than order eight. The initial values for the polynomial coefficients were taken equal to the output parameters of the polynomial fit to the MC simulation of  $\gamma p \rightarrow \pi^0\pi^0 p$ . In the fits to the experimental spectra, the centroid and width of the Gaussian were fixed to the values obtained from the previous fits to the MC simulation for  $\gamma p \rightarrow \omega p \rightarrow \pi^0\gamma p$ , shown in panels (a). This introduced additional restrictions on the background function, improving the separation of the signal and background events. As also seen in Figs. 1-3, the centroid and width of the Gaussian obtained from fitting to the MC simulation of  $\gamma p \rightarrow \omega p \rightarrow \pi^0\gamma p$  suit the experimental  $\omega$  peak very well. This confirms the agreement of the energy calibration and the detector resolution for the experimental data and the MC simulation.

The number of  $\omega \rightarrow \pi^0\gamma$  decays in the experimental  $m(\pi^0\gamma)$  spectra was determined from the area under the Gaussian. For consistency, the detection efficiency in each energy-angle bin was obtained in the same way, i.e., based on a Gaussian fit to the MC simulation for  $\gamma p \rightarrow \omega p \rightarrow \pi^0\gamma p$ , instead of using the number of entries in the  $m(\pi^0\gamma)$  spectra. This approach allowed one to diminish the impact from some deviation of the  $\omega$ -peak

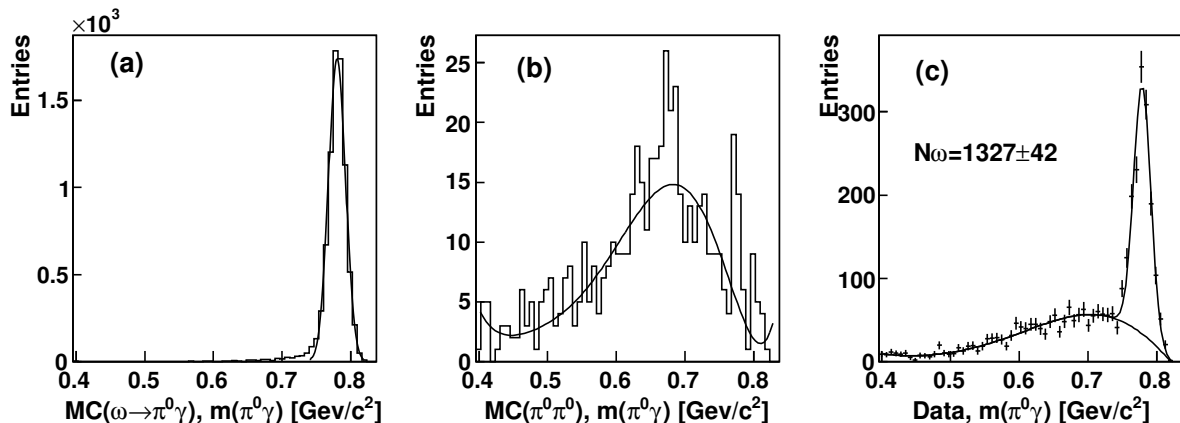


FIG. 2: Same as Fig. 1, but for  $\cos \theta = 0.933$ . A Gaussian fit to the  $\omega$  peak results in  $\sigma = 12.4$  MeV (FWHM=29.2 MeV). A polynomial of order seven used to fit the background.

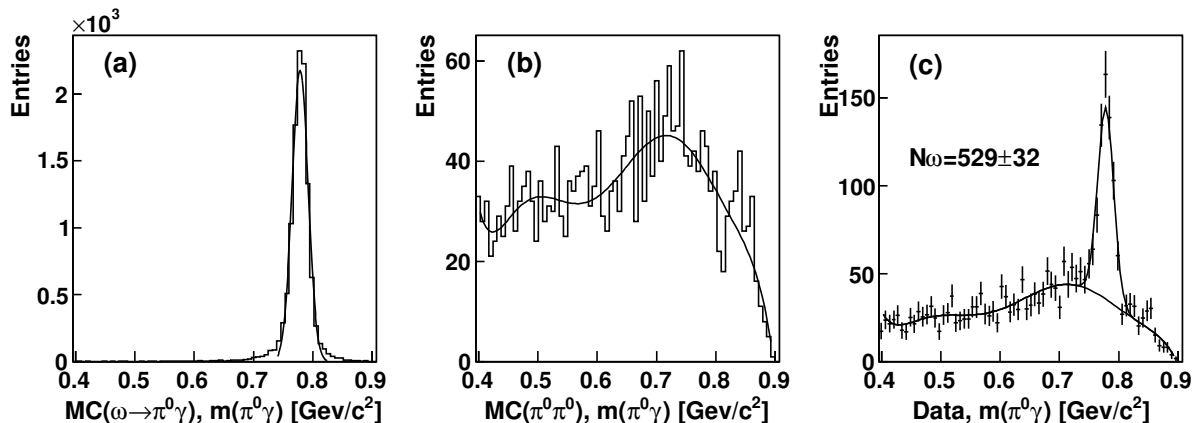


FIG. 3: Same as Fig. 1, but for  $E_\gamma = 1325$  MeV. A Gaussian fit to the  $\omega$  peak results in  $\sigma = 13.6$  MeV (FWHM=32.0 MeV). A polynomial of order eight used to fit the background.

shape from the normal distribution used in the fits.

#### IV. EXPERIMENTAL RESULTS

The total number of  $\omega$  mesons produced in each energy-angle bin was obtained by correcting the number of  $\omega \rightarrow \pi^0\gamma$  decays observed with the corresponding detection efficiency and the  $\omega \rightarrow \pi^0\gamma$  branching ratio (8.28%) from the RPP [2]. The  $\gamma p \rightarrow \omega p$  differential cross sections were obtained by taking into account the number of protons in the target and the photon-beam flux from the tagging facility. Statistical uncertainties of the results were calculated from the errors given by the Gaussian fits. One contribution to the systematic uncertainty comes from the uncertainty in the shape of the background under the  $\omega$  peak and from the deviation of the  $\omega$ -peak shape from the normal distribution. This uncertainty for one energy-angle bin is independent of such uncertainties for other energy-angle bins. The magnitude of this uncertainty, the average of which comprises 6% of individual values in the differential cross sections, was estimated by fulfilling several tests with the experimental and the MC-simulation spectra. For

the experimental data, the fit was repeated with lowering the order of the polynomial used in the fitting procedure and changing the  $m(\pi^0\gamma)$  range fitted. For tests with the MC simulation, the experimental distribution was replaced with the sum of the MC simulations for  $\gamma p \rightarrow \omega p \rightarrow \pi^0\gamma p$  and  $\gamma p \rightarrow \pi^0\pi^0 p$  and fitted as experimental data, checking how well the known number of  $\omega$  events was recovered. Another contribution to the systematic uncertainty, which is practically the same for all energy-angle bins, comes from the determination of the detector acceptance and the photon-beam flux; it was estimated as 5% (see Ref. [23] for more details on this kind of systematic uncertainty).

In Fig. 4, the results of this work for the  $\gamma p \rightarrow \omega p$  differential cross sections are compared to previous measurements at similar energies from SAPHIR [6] and CLAS [13] and to model calculations from Refs. [7, 11]. The vertical error bars shown for all data points in Fig. 4 include statistical uncertainties only. As seen, the data points of this work cover the full production-angle range and have quite small statistical uncertainties. Thus, combining these features of the present results with fairly small energy binning (15 MeV in  $E_\gamma$ ) makes it possible to study the threshold-region dynamics with much better

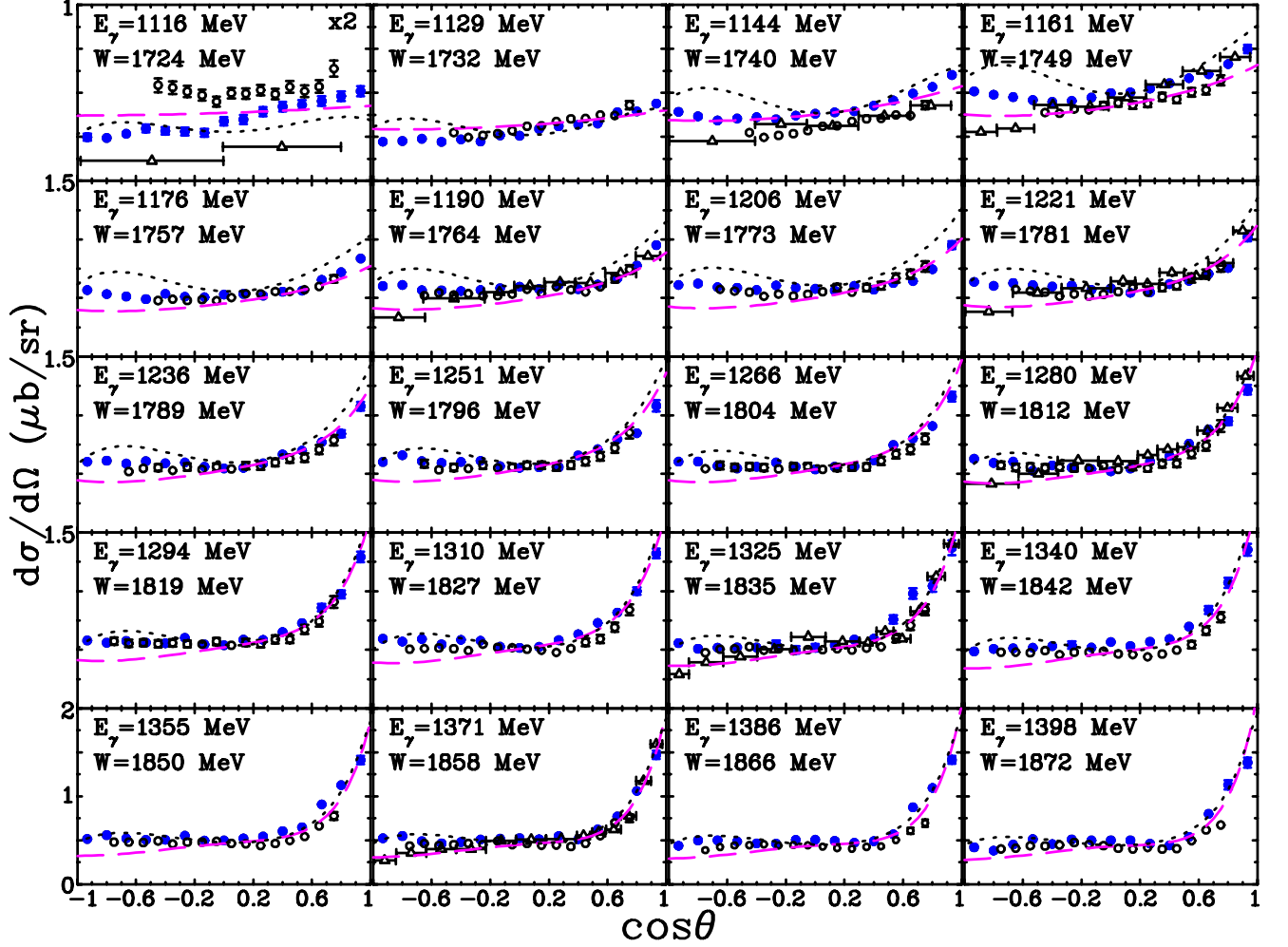


FIG. 4: (Color online) Differential cross sections for  $\gamma p \rightarrow \omega p$  as a function of  $\cos \theta$ , where  $\theta$  is the angle between the directions of the  $\omega$  meson and the incident photon in the c.m. frame. The results of this work are shown by blue dots, SAPHIR [6] results by open triangles, and CLAS [13] results by open circles. The vertical error bars of all data points include statistical uncertainties only. The horizontal error bars are shown only for SAPHIR data, reflecting their nonidentical bins in  $\cos \theta$ . The incident-photon energies of the data points shown for previous experiments are within  $\pm 5$  MeV of  $E_\gamma$  indicated in each panel. Model calculations from Ref. [7] are shown by black short-dashed lines and from Ref. [11] by magenta long-dashed lines.

accuracy than before. As also seen, the present results are in general agreement with previous measurements in the angular range where they overlap. Deviations in absolute values at some energies from the results of CLAS, with general agreement in the angular dependence at the same time, can be explained by a slight difference in  $E_\gamma$ , which can be very important near threshold. The results from SAPHIR for backward angles are smaller than the present and other recent measurements.

The impact of the SAPHIR data on the models can be seen in the calculations from the Giessen group [11], the predictions of which for backward angles follow the behavior of the SAPHIR results. The quark-model calculations from Ref. [7] are in good agreement with the present data at higher energies. At lower energies, the predictions from Ref. [7] are larger than experiment, especially for backward angles. Because the near-threshold amplitudes of this quark model are dominated by the under-threshold states  $N(1720)3/2^+$  and  $N(1680)5/2^+$ ,

the comparison with the present data indicates that the contributions of those two states could be overestimated in Ref. [7].

Near-threshold cross sections of good accuracy allow the extraction of various useful parameters, including resonance masses as well (see, for instance, Refs. [25–27]). In general, the total cross section for an inelastic reaction  $a b \rightarrow c d$  with the particle masses  $m(a) + m(b) < m(c) + m(d)$  can be written as  $\sigma_t = (q/W) \cdot F(W^2)$ , where  $W$  is the c.m. energy and  $q$  is the c.m. momentum of the final-state particles. The factor  $F(W^2)$ , not vanishing at threshold, comes from the sum of production amplitudes squared, and  $(q/W)$  from the integration over the final-state phase space. Because  $W^2$  is linearly related to  $E_\gamma$  for meson photoproduction, the value  $\sigma_t^2$  as a function of  $E_\gamma$  reaches zero at the threshold energy  $E_\gamma = E_\gamma^{\text{th}}$  without any singularity (i.e., linearly, if the final-state  $S$  wave does not vanish at threshold).

The results of this work for  $\sigma_t^2(\gamma p \rightarrow \omega p)$  are shown

as a function of  $E_\gamma$  in Fig. 5(a). In the same figure, the present results are also compared to model calculations from Refs. [7, 11, 12] and to the results from SAPHIR [6], the angular coverage of which (see the horizontal error bars in Fig. 4) was almost full, allowing one to extrapolate the differential cross sections to the full range. The fit of the present  $\sigma_t^2$  data with the formula

$$\sigma_t^2(E_\gamma) = b_1\delta + b_2\delta^2 + b_3\delta^3, \quad (1)$$

with one of four free parameters included in  $\delta = E_\gamma - E_\gamma^{\text{th}}$ , is shown in Fig. 5(a) by a solid red line. For the parameter  $E_\gamma^{\text{th}}$ , the fit results in the value  $(1109.90 \pm 0.82)$  MeV, corresponding to the mass  $m_\omega = (783.10 \pm 0.44)$  MeV/ $c^2$ . It is in good agreement with the RPP value  $m_\omega = (782.65 \pm 0.12)$  MeV/ $c^2$  [2]. Although the estimate made here for the  $\omega$ -meson mass cannot compete in precision with the known RPP value, the agreement observed indicates the good quality of the present data and the correctness of the photon-beam energy calibration, the systematic uncertainty in which was determined as 0.5 MeV [22].

More traditionally, the  $\sigma_t$  behavior of a binary inelastic reaction near threshold can be described as a series of odd powers of  $q$ . The results of this work for  $\sigma_t(q)$  are shown in Fig. 5(b). In the energy range under the study, the formula

$$\sigma_t(q) = a_1q + a_3q^3 + a_5q^5 \quad (2)$$

is enough to describe well the present results for  $\sigma_t(q)$ . The fit of these data with Eq.(2) is shown in Fig. 5(b) by a solid red line, resulting in  $a_1 = (4.42 \pm 0.14) \cdot 10^{-2} \mu\text{b}/(\text{MeV}/c)$ ,  $a_3 = -(1.62 \pm 0.40) \cdot 10^{-7} \mu\text{b}/(\text{MeV}/c)^3$ , and  $a_5 = -(1.14 \pm 2.56) \cdot 10^{-13} \mu\text{b}/(\text{MeV}/c)^5$ . The linear term is determined here by the  $S$  waves only (with the total spin 1/2 and/or 3/2), while the contributions to the cubic term come from both the  $P$ -wave amplitudes and the  $W$  dependence of the  $S$ -wave amplitudes, and the fifth-order term arises from the  $D$  waves and the  $W$  dependences of the  $S$  and the  $P$  waves.

The  $\sigma_t(\gamma p \rightarrow \omega p)$  data near threshold can also be used for determining the  $\omega N$  scattering length  $\alpha_{\omega p}$ , defined by the threshold relation  $d\sigma(\omega p \rightarrow \omega p)/d\Omega|_{\text{th}} = |\alpha_{\omega p}|^2$  (in reality, it is a combination of two independent  $S$ -wave scattering lengths with total spins 1/2 and 3/2). In the VMD framework,  $\alpha_{\omega p}$  appears also in  $\sigma_t(\gamma p \rightarrow \omega p)$  near threshold [28]

$$\sigma_t(\gamma p \rightarrow \omega p)|_{\text{th}} = \frac{q}{k} \cdot \frac{4\alpha\pi^2}{\gamma^2} \cdot |\alpha_{\omega p}|^2, \quad (3)$$

where  $k$  is the c.m. momentum of the incident photon at the  $\gamma p \rightarrow \omega p$  threshold,  $\alpha$  is the fine-structure constant, and  $\gamma = 8.53 \pm 0.14$  is the  $\gamma - \omega$  coupling, as determined from the  $\omega \rightarrow e^+e^-$  decay width [2]. Combining Eq. (3) with the  $a_1$  value from fitting Eq. (2) to the present  $\sigma_t(\gamma p \rightarrow \omega p)$  data results in

$$|\alpha_{\omega p}| = \frac{\gamma}{2\pi} \sqrt{\frac{ka_1}{\alpha}} = (0.82 \pm 0.03) \text{ fm}, \quad (4)$$

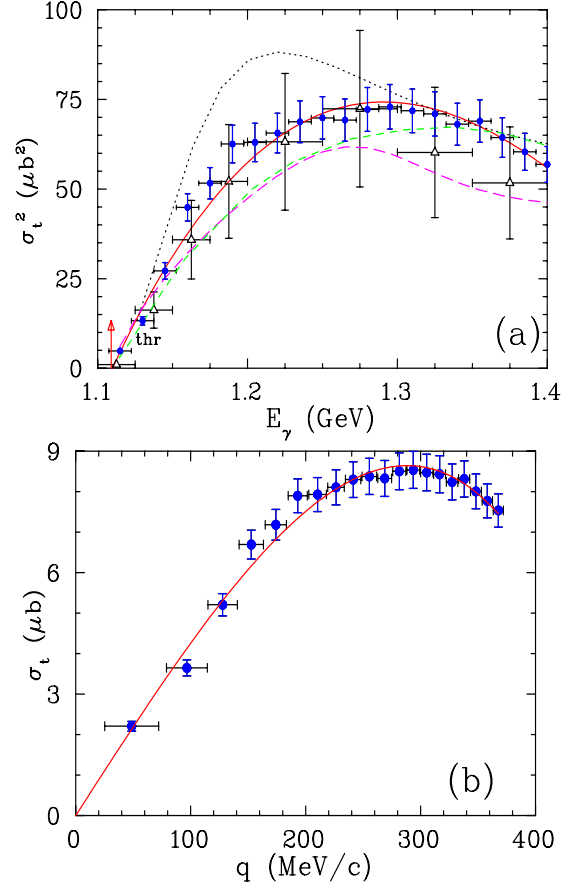


FIG. 5: (Color online) Results of this work (blue dots) for the  $\gamma p \rightarrow \omega p$  total cross sections  $\sigma_t$  are shown in (a) for  $\sigma_t^2$  as a function of the incident-photon energy  $E_\gamma$  and in (b) for  $\sigma_t$  as a function of the c.m. momentum  $q$  of the final-state particles. The  $\sigma_t$  results from SAPHIR [6] are depicted by open triangles. The vertical error bars represent the total uncertainties of the results. The horizontal error bars reflect the energy binning. The red solid line shows the fit of the present data (a) with Eq.(1) and (b) with Eq.(2). The result from the calculation of Ref. [7] is shown by a black short-dashed line, of Ref. [11] by a magenta long-dashed line, and of Ref. [12] by a green dashed line.

which should be considered just as an estimate assuming only the sequence  $\gamma \rightarrow \omega$ ,  $\omega p \rightarrow \omega p$ . A more detailed analysis is needed, however, to exclude contributions from  $\gamma \rightarrow \rho^0$ ,  $\rho^0 p \rightarrow \omega p$ , containing in particular  $\pi^0$  exchange, and from a similar transition  $\gamma \rightarrow \phi$ . Note that the present estimate for  $|\alpha_{\omega p}|$  is within the range defined by other  $\alpha_{\omega p}$  values available in the literature:  $(-0.026 + i 0.28)$  fm from the coupled-channel analysis of the  $\omega$  production in  $\pi N$  and  $\gamma N$  interactions [11],  $(-0.41 \pm 0.05)$  fm from the QCD sum-rule analysis [29],  $(1.6 + i 0.30)$  fm from the effective Lagrangian approach based on chiral symmetry [30], and  $(-0.44 + i 0.20)$  fm from the coupled-channel unitary approach [31]. The dynamical coupled-channel analysis from Ref. [12] yielded separate values for two scattering lengths:  $\alpha_{\omega N}^{1/2} = (-0.0454 - i 0.0695)$  fm and

$\alpha_{\omega N}^{3/2} = (-0.180 - i 0.0597)$  fm, which need to be specially combined for comparing with the effective scattering length obtained directly from the present data.

Existing experimental results for the imaginary [32] and the real [33] parts of the  $\omega$ -nucleus potential were recalculated by one of the present authors (V. M.) into the  $\omega N$  scattering length, using the connection of the meson-nucleus optical potential to the meson-nucleon scattering amplitude described in Ref. [34] (details of these calculations are beyond the scope of the present work and will be published separately). The obtained value,  $\alpha_{\omega N} = (-0.17 \pm 0.40) + i (0.79 \pm 0.11)$  fm, has modulus  $|\alpha_{\omega N}| = (0.81 \pm 0.41)$  fm that turned out to be in agreement, within the uncertainties, with the estimate made in this work.

Availability of good-quality data on  $\omega$  photoproduction near threshold will also allow further analysis of these data for extracting contributions from the pion-exchange and the Born nucleon diagrams. The latter diagrams contain the coupling vertex  $\omega NN$ , which determines the  $\omega$ -exchange contribution to  $NN$  forces and was extracted earlier in the phenomenological analysis of Ref. [35]. Thus, one can check the current understanding of the  $NN$  potential. Threshold data are important here because, at higher energies, the Born contributions decrease and become nonessential with respect to the Pomeron-exchange contribution.

## V. SUMMARY AND CONCLUSIONS

An experimental study of  $\omega$  photoproduction on the proton was conducted by the A2 Collaboration at MAMI. The  $\gamma p \rightarrow \omega p$  differential cross sections are measured from threshold to  $E_\gamma = 1.4$  GeV with 15-MeV binning and full production-angle coverage, improving significantly the data available for this energy range. The quality of the present data near threshold gives access to a variety of physical quantities that can be extracted by

studying the  $\omega N$  system. In particular, our estimate for the  $\omega N$  scattering length is consistent with previous theoretical results, and the estimate of the  $\omega$ -meson mass is in good agreement with the RPP [2] value. The present data are also expected to be invaluable for future partial-wave and coupled-channel analyses, which could provide much stronger constraints on the properties of nucleon states known in this energy range and even reveal new resonances. A partial-wave analysis with extracting spin-density matrix elements from the present data is already in progress, being performed by a theoretical group outside the A2 Collaboration. The results of it will be published later on separately.

## Acknowledgments

We thank T. Barnes, A. B. Gridnev, A. I. Titov, and Q. Zhao for useful remarks and continuous interest in the paper. The authors wish to acknowledge the excellent support of the accelerator group and operators of MAMI. This work was supported by the Deutsche Forschungsgemeinschaft (SFB443, SFB/TR16, and SFB1044), DFG-RFBR (Grant No. 09-02-91330), the European Community-Research Infrastructure Activity under the FP6 “Structuring the European Research Area” programme (Hadron Physics, Contract No. RII3-CT-2004-506078), Schweizerischer Nationalfonds, the UK Science and Technology Facilities Council (STFC 57071/1, 50727/1), the U.S. Department of Energy (Offices of Science and Nuclear Physics, Award Numbers DE-FG02-99-ER41110, DE-FG02-88ER40415, DE-FG02-01-ER41194) and National Science Foundation (Grant No. PHY-1039130, IIA-1358175), INFN (Italy), and NSERC (Canada). Ya. I. Azimov acknowledges support by the Russian Science Foundation (Grant No. 14-22-00281). We thank the undergraduate students of Mount Allison University and The George Washington University for their assistance.

- 
- [1] S. Capstick and W. Roberts, Prog. Part. Nucl. Phys. **45**, S241 (2000).
  - [2] K. A. Olive *et al.*, (Particle Data Group), Chin. Phys. C **38**, 090001 (2014).
  - [3] R. A. Arndt, W. J. Briscoe, I. I. Strakovsky, and R. L. Workman, Phys. Rev. C **74**, 045205 (2006).
  - [4] R. Koniuk and N. Isgur, Phys. Rev. Lett. **44**, 845 (1980).
  - [5] N. M. Kroll, T. D. Lee, and B. Zumino, Phys. Rev. **157**, 1376 (1967); J. J. Sakurai, Phys. Rev. Lett. **22**, 981 (1969).
  - [6] J. Barth *et al.*, Eur. Phys. J. A **18**, 117 (2003).
  - [7] Q. Zhao, Phys. Rev. C **63**, 025203 (2001); private communication, 2013.
  - [8] Y. Oh, A. Titov, and T. S. H. Lee, Phys. Rev. C **63**, 025201 (2001).
  - [9] H. Babacan, T. Babacan, A. Gokalp, and O. Yilmaz, Eur. Phys. J. A **13**, 355 (2002).
  - [10] A. I. Titov and T. S. H. Lee, Phys. Rev. C **66**, 015204 (2002).
  - [11] V. Shklyar, H. Lenske, U. Mosel, and G. Penner, Phys. Rev. C **71**, 055206 (2005); V. Shklyar, private communication, 2013.
  - [12] M. W. Paris, Phys. Rev. C **79**, 025208 (2009).
  - [13] M. Williams *et al.*, Phys. Rev. C **80**, 065208 (2009).
  - [14] A. Willson, Ph.D. Thesis, Florida State Univ. 2013.
  - [15] A. Starostin *et al.*, Phys. Rev. C **64**, 055205 (2001).
  - [16] R. Novotny, IEEE Trans. Nucl. Sci. **38**, 379 (1991).
  - [17] A. R. Gabler *et al.*, Nucl. Instrum. Methods A **346**, 168 (1994).
  - [18] H. Herminghaus *et al.*, IEEE Trans. Nucl. Sci. **30**, 3274 (1983).
  - [19] K.-H. Kaiser *et al.*, Nucl. Instrum. Methods A **593**, 159 (2008).
  - [20] I. Anthony *et al.*, Nucl. Instrum. Methods A **310**, 230 (1991).
  - [21] S. J. Hall *et al.*, Nucl. Instrum. Methods A **368**, 698 (2002).



- (1996).
- [22] J. C. McGeorge *et al.*, Eur. Phys. J. A **37**, 129 (2008).
  - [23] E. F. McNicoll *et al.*, Phys. Rev. C **82**, 035208 (2010).
  - [24] S. Prakhov *et al.*, Phys. Rev. C **79**, 035204 (2009).
  - [25] K. Ackerstaff *et al.*, Phys. Lett. B **389**, 416 (1996).
  - [26] J. Abdallah *et al.*, Eur. Phys. J. C **34**, 127 (2004).
  - [27] A. Nikolaev *et al.*, Eur. Phys. J. A **50**, 58 (2014).
  - [28] A. I. Titov, T. Nakano, S. Date, and Y. Ohashi, Phys. Rev. C **76**, 048202 (2007).
  - [29] Y. Koike and A. Hayashigaki, Prog. Theor. Phys. **98**, 631 (1997).
  - [30] F. Klingl, T. Waas, and W. Weise, Nucl. Phys. A **650**, 299 (1999).
  - [31] M. F. M. Lutz, G. Wolf, and B. Friman, Nucl. Phys. A **706**, 431 (2002); Erratum, **765**, 495 (2006).
  - [32] M. Kotulla *et al.*, Phys. Rev. Lett. **100**, 192302 (2008).
  - [33] S. Friedrich *et al.*, Phys. Lett. B **736**, 26 (2014).
  - [34] E. Friedman and A. Gal, Phys. Rep. **452** 89 (2007).
  - [35] C. Downum, T. Barnes, J. R. Stone, and E. S. Swanson, Phys. Lett. B **638**, 455 (2006).